Guided Noise Reduction for Spectral CT with Energy-Selective Photon Counting Detectors

Michael Manhart, Rebecca Fahrig, Joachim Hornegger, Arnd Doerfler and Andreas Maier

***Abstract*—We investigate the use of joint bilateral filtering for noise reduction in energy-selective photon counting detectors. A guidance image from all energy channels is computed, which steers a non-linear filter to denoise each energy bin individually. Our novel approach is evaluated with cone beam data simulated using a numerical cardiac phantom. Results indicate that the method increases cross-talk between energy channels only at a very slight level. In terms of noise reduction, the method is successful. The rRMSE is reduced by about 60% and the SNR is increased from 3.3 to 72.9 for the channel with the lowest photon count.**

I. Introduction

Spectral CT (S-CT) facilitates the quantitative measurement of material properties in X-ray computed tomography (CT). Popular diagnostic applications are bone removal, measurement of blood volume in the lung or quantification of contrast agent concentrations (e.g., in the myocardium) [1]. S-CT data can be acquired using energy-selective photon counting detectors [2]. The energy-selective detectors assign incoming X-ray photons to energy bins. Figure 1 visualizes an idealized binning of an X-ray photon spectrum into 3 bins. The binned data can be reconstructed separately to obtain volumes with energy-selective attenuation coefficients. This can be utilized, for instance, to reconstruct contrasted and non-contrasted images from a single acquisition. Since iodine contrast agent has a K-edge of 33.2 keV, it will not be visible in high energy bins (e.g., bins around 140 keV) [3]. Because the full spectral data is acquired in one shot, contrasted and non-contrasted images will be perfectly aligned. This is particularly beneficial for imaging of moving organs, e.g., cardiac and lung imaging.

However, by splitting the acquired photons into bins the noise statistics of the corresponding projection images suffer. Especially bins covering only the low energy portion of the spectrum energy distribution are corrupted by noise. For instance, Figure 2a shows a numerical projection image of the spectral data corresponding to Bin 1 in Figure 1. Due to the low energy of this bin with respect to the spectrum distribution, the projection image is obviously noisy. Thus an expedient noise reduction method is required to obtain appropriate image quality at clinically acceptable dose levels.

Iterative reconstruction algorithms have shown superior image quality [4], but suffer from high computational demand. Alternative computationally faster methods have been proposed, which apply adaptive, anisotropic filters in a preprocessing step on the projection data [5] or in a post-processing step on reconstructed images [6], [7]. The advantage of projection space denoising is that for photon counting detectors the noise can be modeled accurately and easily using Poisson statistics. Up to now, projection space denoising methods using noise adaptive filter kernels [5], [8], [9], as well as methods using edge preserving filters [10] and combinations of both methods [11] have been presented.

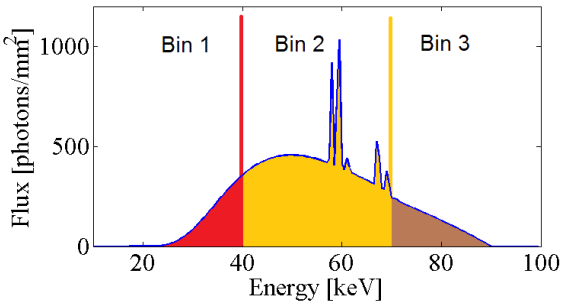

Figure 1: Binning of a X-ray spectrum into 3 bins.

In this work we extend the idea of projection based denoising by edge preserving filtering to S-CT data of energy-selective detectors. We guide the edge preserving filter using information from the fully acquired spectrum. The novel approach is evaluated using the CONRAD cone beam reconstruction and simulation framework [12] with data from a numerical cardiac phantom.

II. Methods

A. Energy-Selective Detector

The energy-selective photon counting detector assigns incoming photons into $b = 1 \dots B$ bins. Each bin covers a spectral bandwidth of ΔE and the spectral bandwidth of the first bin starts at energy level E^0. Let $\mathbf{x} = (u, v)$ be the spatial location of the detector pixel with column index u and row index v. The expected photon count $I_b(\mathbf{x})$ measured for bin b at location $\mathbf{x}$ is given by

$$I_b(\mathbf{x}) = I^0 \int_{E^0+(b-1)\Delta E}^{E^0+b\cdot\Delta E} S(E) \exp\left(-\int_{L(\mathbf{x})} \mu\,(E,l)\ \mathrm{d}l\right) \mathrm{d}E, \tag{1}$$

where I^0 denotes the number of photons per mm^2 arriving at the detector in the unattenuated case and $S\,(E)$ denotes the spectral distribution with the area under the curve normalized

A. Maier, J. Hornegger, and M. Manhart are with Pattern Recognition Lab, Department of Computer Science, Friedrich-Alexander-Universität Erlangen-Nürnberg, Germany. M. Manhart and A. Doerfler are with Department of Neuroradiology, Universitätsklinikum Erlangen, Erlangen, Germany. R. Fahrig is with Department of Radiology, Stanford University, CA, USA. J. Hornegger is with Erlangen Graduate School in Advanced Optical Technologies (SAOT).
Email: andreas.maier@cs.fau.de

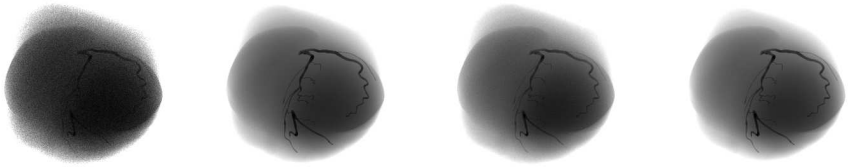

(a) Bin 1 (b) Bin 2 (c) Bin 3 (d) Guidance image

Figure 2: Energy-selective projection images and guidance image for joint bilateral filtering.

to one. The X-ray attenuation is defined by $\mu(E, l)$ and depends on the photon energy E and the spatial position l on the line $L(\mathbf{x})$, which points from the X-ray source to the detector pixel $\mathbf{x}$. Accordingly, the log-transformed image $P_b(\mathbf{x})$ is given by

$$P_b(\mathbf{x}) = -\log \frac{I_b(\mathbf{x})}{I_b^0} \text{ with } I_b^0 = \int_{E^0+(b-1)\Delta E}^{E^0+b\cdot\Delta E} I^0 S(E)\,\mathrm{d}E. \tag{2}$$

B. Joint Bilateral Filtering

For guided edge preserving noise reduction we apply joint bilateral filtering (JBF) [13]. The JBF is a variant of the bilateral filter [14], where the edge preservation is controlled by a guidance image. Each intensity of a filtered image $P'(\mathbf{x})$ is computed as a weighted average of the intensities of the original image $P(\mathbf{x})$ in a spatial neighborhood $\mathcal{N}_\mathbf{x}$

$$I'(\mathbf{x}) = \frac{\sum\limits_{\mathbf{o}\in\mathcal{N}_\mathbf{x}} I(\mathbf{x}+\mathbf{o})\mathcal{W}(\mathbf{x},\mathbf{o})}{\sum\limits_{\mathbf{o}\in\mathcal{N}_\mathbf{x}} \mathcal{W}(\mathbf{x},\mathbf{o})}, \tag{3}$$

$$\text{with } \mathcal{W}(\mathbf{x},\mathbf{o}) = \mathcal{G}_{\sigma^\mathrm{S}}(\mathbf{x}-\mathbf{o})\cdot\mathcal{G}_{\sigma^\mathrm{R}}\left(I^\mathrm{G}(\mathbf{x}) - I^\mathrm{G}(\mathbf{x}+\mathbf{o})\right),$$

where $\mathcal{G}_\sigma(\mathbf{z}) = \exp\left(-0.5\cdot\|\mathbf{z}\|_2^2/\sigma^2\right)$ denotes a Gaussian kernel. The weighting term $\mathcal{W}$ consists of the spatial closeness term $\mathcal{G}_{\sigma^\mathrm{S}}$ controlled by the domain parameter σ^S and the range similarity term $\mathcal{G}_{\sigma^\mathrm{R}}$ controlled by the range parameter σ^R and by the guidance image I^G.

C. Guided Range Filtering

To exploit the complete spectral information for the edge preservation, the guidance image is formed by the sum over all spectral bins. Therefore the guidance image to filter the binned projection images $I_b(\mathbf{x})$, $b = 1\ldots B$ is defined by

$$I^\mathrm{G}(\mathbf{x}) \quad = \quad \sum_{b=1}^{B} I_b(\mathbf{x}) \tag{4}$$

Note that the summation inherently includes an uncertainty weighting as the signal-to-noise ratio is proportional to the number of measured photons. The range parameter σ^R is set to the minimal contrast difference D in the guidance image, which should be preserved.

D. Guided Filtering in Reconstruction Domain

The idea of JBF can also be applied after reconstruction of the image. In this case, however, the guidance image cannot be simply created by a sum of the individual reconstructed volumes $f_b(\mathbf{y})$. Note that $\mathbf{y} = (x, y, z)$ is used to index the volume space. In order to create a suitable guidance image, the image contributions have to be scaled according to their reliability. In our case, we picked an inverse variance weighting and denote the variance in bin b with σ_b^2. This leads to the following guidance image

$$f^\mathrm{G}(\mathbf{y}) = \sum_{b=1}^{B} \frac{f_b(\mathbf{y})}{\sigma_b^2}. \tag{5}$$

As this method operates in the image domain (ID), we refer to it as ID-JBF.

E. Experimental Setup

We simulated a static instance of the human heart as described in [15]. The contents of the heart chambers were simulated as water with a density of 1.06. The heart muscle was simulated as water with a density of 1.05. In addition, the coronary arteries were filled with a solution of Iopromide ($C_{18}H_{24}I_3N_3O_8$) that contained $0.76\,\mathrm{g}$ of contrast agent per gram of water. The density of this solution was set to 1.40 g/cm^3 which is typical for a clinical contrast agent (e.g., Ultravist© 370). The simulated spectrum is shown in Fig. 1. Its properties were adjusted such that its half-value-layer is comparable to that of a clinical C-arm system. We set the tube voltage to $90\,\mathrm{kVp}$ and the time-current product to $0.1\,\mathrm{mAs}$. In this configuration, we have $I_1^0 = 948$, $I_2^0 = 28982$, and $I_3^0 = 10103$ photons per mm^2 arriving at each detector bin, if no object is hit between source and detector. In the present experiment, we did not simulate cross-talk between the energy bins and the detection efficiency was 100% at all energies. While this might not be the case in a real detector, it maximizes the independence between the energy bins and allows us to study correlations between the energy bins that are introduced by the denoising method. We did not perform an optimization of the energy thresholds in the present study to maximize the iodine contrast, as the focus of the study is denoising and not material separation. The bins were equally spaced between 10 and 100 keV according to the sampling range of the spectrum, i.e., $E^0 = 10\,\mathrm{keV}$ and $\Delta E = 30\,\mathrm{keV}$. All simulations and algorithms were created using our open-source

flat panel simulation and reconstruction framework CONRAD [12].

JBF filtering was performed in intensity space before conversion to line-integral space. The intensity difference in the contrast filled vessels D was found to be 1000 in the guidance image. We picked $\sigma^{\mathrm{S}} = 9$ and $\sigma^{\mathrm{R}} = 100$ for the projection-based filtering. Then a standard Feldkamp short-scan reconstruction was performed using a Shepp-Logan filter [16]. We simulated 495 projections over an angular range of 200 degrees, which is the short-scan range of our 620×480 detector. Detector element size was $0.6\times0.6\,\mathrm{mm}^2$, the source detector distance $1200\,\mathrm{mm}$, and the source to center of rotation distance was $750\,\mathrm{mm}$. The heart fit all projections in all views, thus no truncation correction had to be performed. After reconstruction onto an 256^3 image grid with $0.5\times0.5\times0.5\,\mathrm{mm}^3$ voxels, we investigated the use of ID-JBF. Here, we chose the parametrization as $\sigma^{\mathrm{S}} = 5$ and $\sigma^{\mathrm{R}} = D$. The guidance image weightings σ_b^2 where determined by estimating the noise variance inside homogenous regions of the corresponding reconstructed images. JBF filtering and back-projection was implemented in OpenCL.

Errors were measured using structural similarity [17], linear correlation coefficient, and the relative root means square error (rRMSE), that is the RMSE scaled by the maximum intensity.

III. Results

Table I displays structural similarity and correlations between the different reconstruction approaches. All denoising methods show improved results compared to the ground truth. While correlations increase slightly, the structural similarity between the three bins is preserved by all methods. Thus, we can conclude that the JBF does not cause the three energy bins to display identical information.

Figure 3 shows the center slices of the different reconstructions of Bin 1. All reconstructions are shown at the same window and level [10, 110 HU]. The ground truth image (Figure 3a) nicely differentiates between the heart chambers and the heart muscle. The excessive noise in Bin 1 does not permit differentiation of the two heart chambers (Figure 3b, rRMSE 3.10%, SNR 3.3). JBF filtering in the projection domain allows visualization of a slight contrast between the two heart chambers. Streaking from polychromatic effects is emphasized (Figure 3c, rRMSE 1.33%, SNR 29.0). ID-JBF only is not able to recover the separation between the heart chambers and the muscle tissue (Figure 3d, rRMSE 1.20%, SNR 47.6). Additional filtering in the image domain reduces noise and streak artifacts further (Figure 3e, rRMSE 1.26 %, SNR 72.3).

IV. Discussion

We applied the idea of joint bilateral filtering to energy-resolving detectors. First results demonstrate that the method is feasible. We were able to restore low-contrast image data in a very noisy channel. The comparisons between the channels showed that the method introduces very little cross-talk between the different energy bins, and their similarity is only slightly increased.

An advantage of bilateral filters is that they are very easy to configure. We require only two parameters which can be easily obtained from the guidance image. The first one is σ^{S} which controls the locality of desired smoothing. It can be chosen in the same way as a normal Gaussian filter. The second parameter σ^{R} describes the amount of edge preservation. A good rule-of-thumb way of setting it is to measure the lowest contrast from the image that needs to be preserved (D). In case of projection-based filtering, however, we recommend setting σ^{R} to 10% to 20% of this value, as the preservation of very small signal changes at the edge of high contrast contours is crucial. Otherwise, streaking artifacts can arise in the reconstructed images. In our present study, we already introduced such slight streaking.

At present, we only investigated JBF and did not include further modifications such as ray-by-ray weighting [5], [9] or projection stack filtering [8]. Integration of both techniques into this method is straight-forward, as the filter kernel is designed for each ray individually anyway. Thus, we would expect only minor increases in terms of run time. However, this will require a different object, as we did not observe strong streak noise in our reconstructions. Another topic for future work is the straight-forward extension of JBF in the image domain to 3D.

V. Conclusions

We created a joint bilateral filter for energy-selective detectors. First results are encouraging. We found that only little cross-talk is introduced between the channels. The SNR was improved from 3.3 to 72.3 while preserving a low rRMSE error.

Acknowledgments

The authors gratefully acknowledge funding of the Medical Valley national leading edge cluster, Erlangen, Germany, diagnostic imaging network, sub-project BD 16, research grant nr. 13EX1212G.

References

[1] M. Balda, "Quantitative Computed Tomography," Ph.D. dissertation, Friedrich-Alexander-Universität Erlangen-Nürnberg, 2011.

[2] D. Niederlohner, F. Nachtrab, T. Michel, and G. Anton, "Using the Medipix2 detector for photon counting computed tomography," in *Nuclear Science Symposium Conference Record*, vol. 4. IEEE, 2005, pp. 2327–2331.

[3] N. Maaß, S. Sawall, M. Knaup, and M. Kachelrieß, "Dose minimization for material-selective CT with energy-selective detectors," in *Nuclear Science Symposium and Medical Imaging Conference (NSS/MIC)*. IEEE, 2011, pp. 4447–4452.

[4] J.-B. Thibault, K. D. Sauer, C. A. Bouman, and J. Hsieh, "A three-dimensional statistical approach to improved image quality for multislice helical CT," *Medical Physics*, vol. 34, no. 11, pp. 4526–4544, 2007.

[5] M. Kachelrieß, O. Watzke, and W. A. Kalender, "Generalized multi-dimensional adaptive filtering for conventional and spiral single-slice, multi-slice, and cone-beam CT," *Medical Physics*, vol. 28, no. 4, pp. 475–490, 2001.

[6] H. Bruder, R. Raupach, J. Sunnegardh, M. Sedlmair, K. Stierstorfer, and T. Flohr, "Adaptive iterative reconstruction," in *SPIE Medical Imaging*, vol. 7961, 2011, pp. 79 610J–1 79 610J–12. [Online]. Available: http://dx.doi.org/10.1117/12.877953

[7] Z. Li, L. Yu, J. D. Trzasko, J. G. Fletcher, C. H. McCollough, and A. Manduca, "Adaptive non-local means filtering based on local noise level for CT denoising," in *SPIE Medical Imaging*. International Society for Optics and Photonics, 2012, pp. 83 131H–83 131H.

Image	GT Bin 1	GT Bin 2	GT Bin 3	Bin 2	Bin 3
Ground truth (GT) Bin 1	1.0 (1.0)	0.78 (0.97)	0.62 (0.99)	0.78 (0.97)	0.62 (0.99)
No Filtering Bin 1	0.95 (0.91)	0.67 (0.87)	0.52 (0.91)	0.69 (0.90)	0.56 (0.92)
JBF Bin 1	0.98 (0.98)	0.76 (0.95)	0.60 (0.98)	0.79 (0.99)	0.64 (0.99)
ID-JBF Bin 1	0.98 (0.98)	0.75 (0.95)	0.60 (0.98)	0.78 (0.98)	0.64 (0.99)
JBF + ID-JBF Bin 1	0.98 (0.98)	0.76 (0.65)	0.60 (0.98)	0.79 (0.99)	0.64 (0.99)

Table I: Structural similarity and linear correlation (in brackets) for the different reconstruction methods. All JBF combinations deliver significant improvements compared to the baseline reconstruction (No Filtering Bin 1) in terms of noise reduction. Visual inspection of ID-JBF, however, demonstrates that it is not able to preserve the low-contrast difference between heart chambers and muscle (cf. Figure 3d).

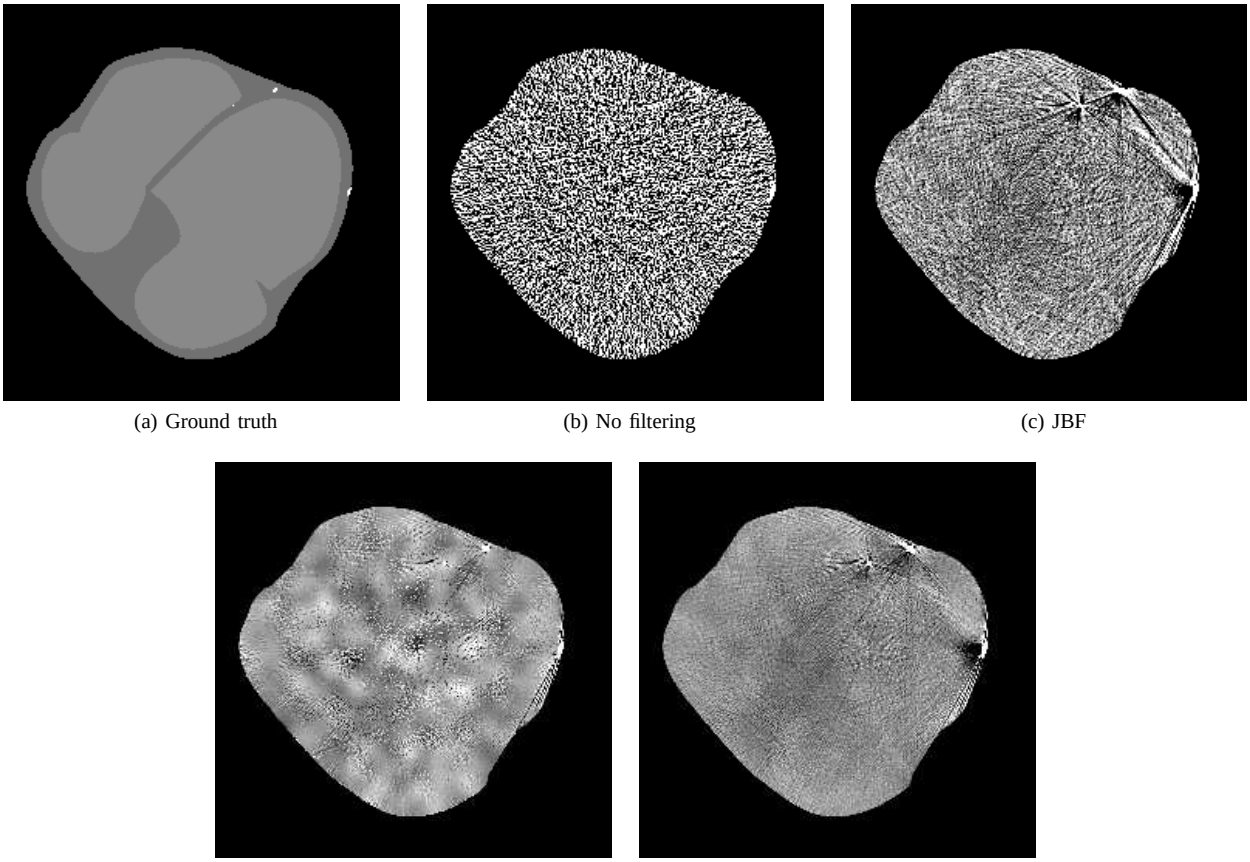

(a) Ground truth (b) No filtering (c) JBF

(d) ID-JBF (e) JBF + ID-JBF

Figure 3: Comparison between the different reconstruction methods in the central slice of Bin 1 [10, 110 HU].

[8] A. Maier, L. Wigström, H. Hofmann, J. Hornegger, L. Zhu, N. Strobel, and R. Fahrig, "Three-dimensional anisotropic adaptive filtering of projection data for noise reduction in cone beam CT," *Medical Physics*, vol. 38, no. 11, pp. 5896–5909, 2011. [Online]. Available: http://www5.informatik.uni-erlangen.de/Forschung/Publikationen/2011/Maier11-TAA.pdf

[9] G. L. Zeng and A. Zamyatin, "A filtered backprojection algorithm with ray-by-ray noise weighting," *Medical Physics*, vol. 40, no. 3, pp. 031 113–1–7, 2013.

[10] A. Manduca, L. Yu, J. D. Trzasko, N. Khaylova, J. M. Kofler, C. M. McCollough, and J. G. Fletcher, "Projection space denoising with bilateral filtering and CT noise modeling for dose reduction in CT," *Medical Physics*, vol. 36, no. 11, p. 4911, 2009.

[11] L. Yu, A. Manduca, M. Jacobsen, J. D. Trzasko, J. G. Fletcher, D. R. DeLone, and C. H. McCollough, "Adaptive modulation of bilateral filtering based on a practical noise model for streaking and noise reduction in multi-slice CT," in *Proc SPIE Medical Imaging*, vol. 7622, 2010, p. 76222O.

[12] A. Maier, H. Hofmann, M. Berger, P. Fischer, C. Schwemmer, H. Wu, K. Müller, J. Hornegger, J.-H. Choi, C. Riess, A. Keil, and R. Fahrig, "CONRAD - A software framework for cone-beam imaging in radiology," *Medical Physics*, vol. 40, no. 11, pp. 111 914–1–8, 2013.

[13] G. Petschnigg, R. Szeliski, M. Agrawala, M. Cohen, H. Hoppe, and K. Toyama, "Digital photography with flash and no-flash image pairs," *ACM Transactions on Graphics (TOG)*, vol. 23, no. 3, pp. 664–672, 2004.

[14] V. Aurich and J. Weule, "Non-linear Gaussian filters performing edge preserving diffusion," in *Mustererkennung 1995*, ser. Informatik aktuell, G. Sagerer, S. Posch, and F. Kummert, Eds. Springer Berlin Heidelberg, 1995, pp. 538–545.

[15] A. Maier, H. G. Hofmann, C. Schwemmer, J. Hornegger, A. Keil, and R. Fahrig, "Fast simulation of X-ray projections of spline-based surfaces using an append buffer," *Physics in Medicine and Biology*, vol. 57, no. 19, pp. 6193–6210, 10 2012.

[16] G. L. Zeng, *Medical image reconstruction: A conceptual Tutorial*, 1st ed. Berlin, Germany: Springer, 2010.

[17] Z. Wang, A. Bovik, H. Sheikh, and E. Simoncelli, "Image quality assessment: from error visibility to structural similarity," *Image Processing, IEEE Transactions on*, vol. 13, no. 4, pp. 600–612, April 2004.